END
DATE
FILMED
84
DTIC

ETL-0345

A test strategy for high resolution image scanners

Armin W. Gruen

Ohio State University
1958 Neil Ave.
Columbus, OH 43210

OCTOBER 1983

DTIC
S ELECTE
NOV 28 1983
D
D

Prepared for

83 11 28 014

SECURITY CLASSIFICATION OF THIS PAGE *(When Data Entered)*

REPORT DOCUMENTATION PAGE		READ INSTRUCTIONS BEFORE COMPLETING FORM
1. REPORT NUMBER ETL-0345	**2. GOVT ACCESSION NO.** AD-A134 998	**3. RECIPIENT'S CATALOG NUMBER**
4. TITLE *(and Subtitle)* A Test Strategy for High Resolution Image Scanners		**5. TYPE OF REPORT & PERIOD COVERED** Final Technical Report (13 Mar 1983 to 15 Sept 1983)
		6. PERFORMING ORG. REPORT NUMBER OSU/DGSS-350
7. AUTHOR(s) Armin W. Gruen		**8. CONTRACT OR GRANT NUMBER(s)** DAAG29-81-D-0100
9. PERFORMING ORGANIZATION NAME AND ADDRESS Department of Geodetic Science and Surveying The Ohio State University 1958 Neil Ave., Columbus, OH 43210		**10. PROGRAM ELEMENT, PROJECT, TASK AREA & WORK UNIT NUMBERS**
11. CONTROLLING OFFICE NAME AND ADDRESS U.S. Army Engineer Topographic Laboratories Fort Belvoir, VA 22060		**12. REPORT DATE** October 1983
		13. NUMBER OF PAGES
14. MONITORING AGENCY NAME & ADDRESS *(if different from Controlling Office)* Battelle Columbus Laboratories 200 Park Drive - P.O. Box 12297 Research Triangle Park, NC 27709		**15. SECURITY CLASS.** *(of this report)* UNCLASSIFIED
		15a. DECLASSIFICATION/DOWNGRADING SCHEDULE

16. DISTRIBUTION STATEMENT *(of this Report)*

Approved for public release; distribution unlimited

17. DISTRIBUTION STATEMENT *(of the abstract entered in Block 20, if different from Report)*

18. SUPPLEMENTARY NOTES

19. KEY WORDS *(Continue on reverse side if necessary and identify by block number)*

High Resolution Image Scanner	MTF
Geometrical and radiometric performance	Dynamic range, linearity, noise
Dynamic scanning errors	Response uniformity
Skewness of array line	Flare light, coherency effects
Length and linearity of array line	Temporal stability

20. ABSTRACT *(Continue on reverse side if necessary and identify by block number)* The scope of this study is the design of a device-independent test strategy for performance tests of the AIDS (Advanced Image Digitizing System) scanner. Major system characteristics to be tested are the geometrical accuracy, linearity of gray shade response, MTF, and resolution of the output. Other parameters addressed here are dynamic range, noise, response uniformity, flare light, coherency, and temporal stability. Test standards are suggested and data processing aspects are considered for both the geometric and radiometric tests. The recommended test strategy is finally summarized in table format.

DD FORM _{1 JAN 73} 1473 EDITION OF 1 NOV 65 IS OBSOLETE

A TEST STRATEGY FOR HIGH RESOLUTION IMAGE SCANNERS

by

Armin W. Gruen
Department of Geodetic Science and Surveying
The Ohio State University
1958 Neil Avenue
Columbus, Ohio 43210

Prepared for

Accession For	
NTIS GRA&I	X
DTIC TAB	☐
Unannounced	☐
Justification	
By	
Distribution/	
Availability Codes	
Avail and/or	
Dist Special	
A/l	

The views, opinions, and/or findings contained in this report are those
of the author(s) and should not be construed as an official Department of
the Army position, policy, or decision, unless designated by other docu-
mentation.

PREFACE

The author is particularly grateful to Professor P.N. Slater, Optical Sciences Center, University of Arizona, for his valuable advice. Dr. Slater acted as a consultant on this project and contributed the section on the radiometric performance tests.

TABLE OF CONTENTS

LIST OF FIGURES

A TEST STRATEGY FOR HIGH RESOLUTION IMAGE SCANNERS

1. Introduction

The scope of this study is the design of a device independent test strategy for performance tests of the AIDS (Advanced Image Digitizing System) scanner. Major system characteristics to be tested are the geometrical accuracy, linearity of gray shade response, MTF, and resolution of the output. The study is of a purely conceptual type, yet most of the procedures suggested here have proven their practical potential elsewhere. The major performance parameters of the AIDS are described in AIDS (1982). The input material is photographic film. The AIDS shall be capable of scanning over a maximum format of 9.5" x 9.5". The minimum scanned image size shall be 1024 x 1024 pixels. The scanning resolution shall be 100 line pairs per millimeter over a format of 6.6" x 6.6" at a MTF level of 0.3. As a secondary requirement the AIDS shall scan the full format at larger pixel sizes, corresponding to a resolution of 70, 50, and 33 line pairs per millimeter, at a MTF level of 0.3. The relative geometric positional accuracy of the output shall be one pixel mean square error over the entire 9.5" x 9.5" format.

The system shall provide two scanning dynamic ranges; a range spanning 1.25 density units and a range spanning 2.50 density units. Pixels shall be generated in both a 8-bit and a 11-bit mode. The 8-bit mode shall produce data having 255 equidensity steps with one step repeatability. Linearity shall be maintained within 0.02 density units or one percent of the scanning density range, whichever is greater. The 11-bit "intensity" mode shall produce 1023 equi-intensity steps with eight steps repeatability. The linearity shall be maintained within 0.5 percent of the scanning intensity range.

The highest average scanning rate of the system shall be not less than 2 Mega Pixels per second.

The tests in this study are designed such that they can be performed "in situ", i.e. with the test standards placed on the film holder and with all relevant system components in their normal position of operation.

The structure of this report distinguishes clearly between tests of the geometric and the radiometric performance. Both parameters, the geometric and the radiometric accuracy, however, are closely related in practice. A defect in the radiometric performance of an electro-optical element might well influence positional measurements. The geometric resolution is dependent on the radiometric resolution and vice versa. The MTF determination with multiple-bar targets across scan direction might be disturbed by tracking errors of the film holder.

Chapter 2 deals with the geometric performance. Following the discussion of some possible instrument errors a number of test standards is suggested for use in the test procedures. The description of these test procedures, together with some aspects of data processing and data analysis concludes Chapter 2.

The radiometric performance tests are depicted in Chapter 3. Particularly touched upon are MTF measurement, dynamic range, linearity and noise, response uniformity, flare light, temporal stability, and coherency effects.

Chapter 4 summarizes the test procedures in table format and indicates options and priorities.

2. Test of the Geometrical Performance

The image scanner produces a digital image of the scanned analog
film image. The geometric performance describes the degree of closeness
(geometric fidelity) between the analog and the digital image (input
versus output). In order to check this closeness, test patterns of known
form and dimension have to be scanned. A comparison between the input
pattern and the output pattern shows the geometric performance of the
scanner. The major problems here are the design of suitable test pat-
terns ("test standards"), the development of test procedures and data pro-
cessing methods. The tests of the geometrical per mance can be formu-
lated such that they are resolution independent.   ly the dimensions of
the test standards must be selected such that they .low for sufficient
responses at all resolution levels. Critical for   .·rcessful geometrical
test is the design of these test standards. Test · .ards are usually
constructed such that they allow for the detection of any expected instru-
ment errors. Since the constructional details of the AIDS are not known
at this point, the instrument errors which might cause geometrical defor-
mations cannot be predicted in advance. A thorough analysis of all ex-
pected instrument errors is not feasible at this stage. The test stand-
ards are selected in a general way such that they allow for the detection
of possible instrument errors. Some possible instrument errors are de-
scribed in the following chapter. Most of these errors assume a linear
array to be used for scanning. If this does not apply the correspondingly
designed tests are not relevant.

2.1 Some possible instrument errors

In the following discussion we will assume that the scanner consists
of a linear array of a (variable) number e (e = 1, ..., n) photosensi-
tive elements.

ℓ_a = length of array

linear array (e elements)

ℓ_a

scan direction   (center line)
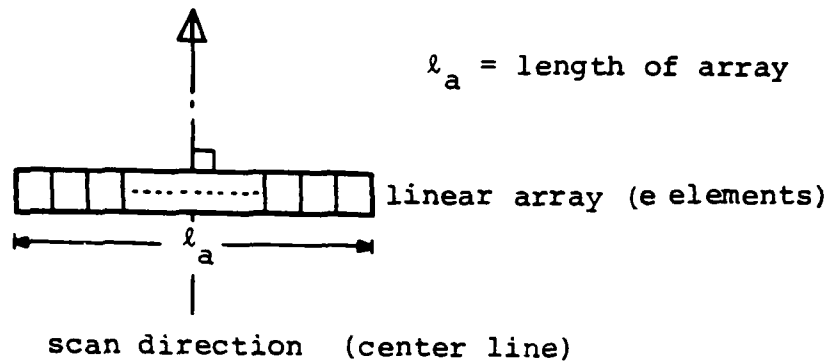
Figure 1: Linear array, mounted perpendicular to scan direction

2.1.1. Dynamic errors in straight line scanning

Hoehle (1983) describes three major types of errors in straight line plotting (Figure 2).

waviness

stepping

tracking
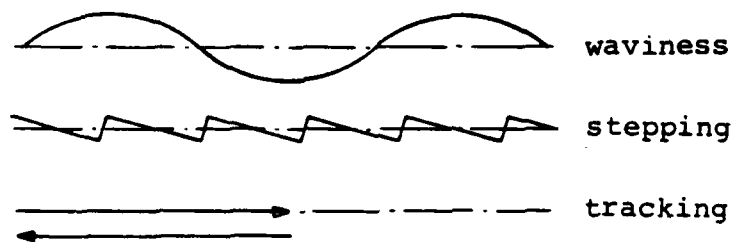
Figure 2: Major errors in straight line plotting
(according to Hoehle (1983))

Similar errors can be expected in a general scanning process. Waviness and stepping are due to mechanical oscillations and deformations and to

the increment size. Stepping should only appear if the scanning lines
are inclined to the driver's axes, which is not likely to be the case
in the AIDS. Waviness and tracking errors however might emerge in any
scanning system. Tracking errors could show up as an interval error
Δd when the transition from one line to another is made (Figure 3 a) or/
and as a convergence/divergence of the supposedly parallel scan lines
(Figure 3 b). The size of the tracking errors Δd, γ might even change
from one line pair to another.

    a) interval error   b) convergence error
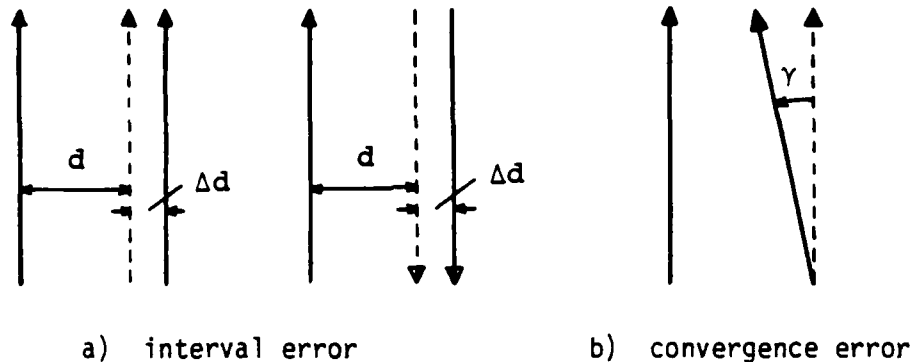
Figure 3: Tracking errors

Besides causing geometrical displacements, waviness and tracking errors
might produce gaps in coverage or oversampling in and/or across scan direc-
tion.

2.1.2. Skewness of array line

Conceptually the linear array is mounted perpendicularly to the
direction of scan (Figure 3 a). The scan interval d is thus equal to
the length of the array ℓ_a. A skewness of the array relative to the
scan line might cause gaps in the scan coverage (Figure 4 b).
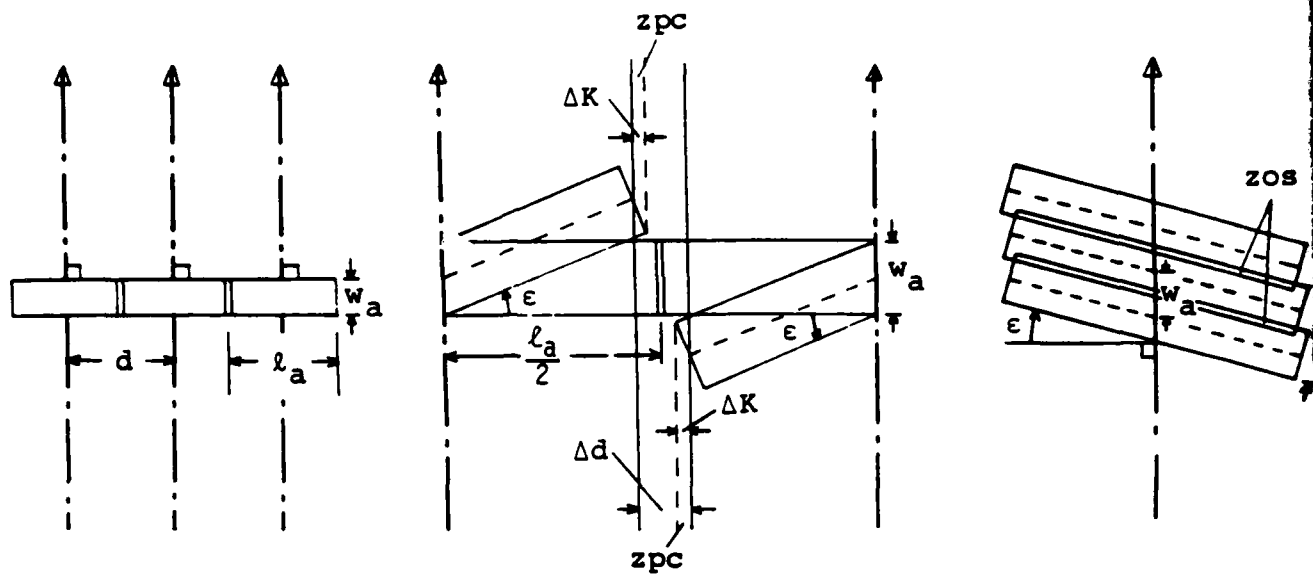
a) correct mount b) mounting error ε, caus- c) mounting error ε,
                      ing gaps across scan   causing oversampling
                      direction   in scan direction

<u>Figure 4</u>: Skewness of array line

   w_a = scanner width $\hat{=}$ advancement of scanner

   zpc ... zones of partial coverage

   zos ... zones of oversampling

Certain zones (zpc) are only covered by a portion of an array element.
The width of the zone of partial coverage is

$$2\Delta K = w_a \sin\varepsilon \quad .$$

The interval error Δd is

$$\Delta d = \ell_a (1 - \cos\varepsilon) \quad .$$

A gap in coverage results if

$$\Delta d > 2\Delta K \quad ,$$

or $\quad \ell_a (1 - \cos\varepsilon) > w_a \sin\varepsilon$,

$$\tan \frac{\varepsilon}{2} > \frac{w_a}{\ell_a} \quad .$$

For a small ε we get the condition

$$\varepsilon > \frac{2w_a}{\ell_a} \quad .$$

A loss of information, however, might occur for even smaller mounting errors ϵ, because along zpc the size of the effective array area is reduced. Oversampling might take place along the zones zos (compare Figure 4 c).

2.1.3. Length of array line

According to tests conducted at Messerschmidt, Boelkow, Blohm (O. Hofmann, personal communications) linear arrays of about 20 mm length showed approximately ±10 µm deviation from their correct length. This deviation can be corrected during the scanner calibration process. Remaining deficiencies in the length of the array line would cause gaps or overlap in the output.

2.1.4. Linearity of array line

According to O. Hofmann (personal communications), the misalignment of CCD array elements is generally negligible. A misalignment would produce "sheared" images, like the example in Figure 5.

original   sheared image
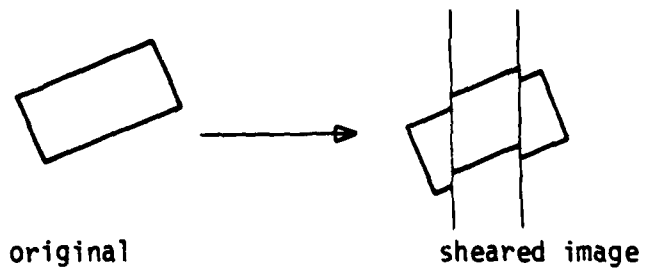
Figure 5: Sheared image caused by array element misalignment

Misalignment could result in an overall deformation of the line (Figure 6 a) or could show up as a sporadic displacement of one or more elements (Figure 6 b).

a) Overall deformation
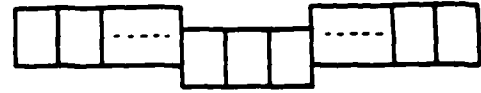
b) Displacement of a set of elements

Figure 6: Types of misalignment

2.1.5. Sampling rate errors in scan direction

If the sampling rate is not adjusted to the physical length of the pixel in scan direction and/or if any constant differences between these two parameters are not considered in the definition of the pixel location , a geometrical distortion in scan direction would result. In the simplest case of constant difference an affine deformation would ensue.

2.1.6. Other system errors

Some additional errors which might occur in the system are

- expansion and creep of the optical system generated by the heat of the light source
- motion of film caused by vibrations at high scanning speeds
- non-orthogonality of film holder to the optical axis
- flatness of film with respect to holder
- relief of film/emulsion.

These errors are not easily separable, but like the others they are part of the overall error budget.

2.2. Test standards and test patterns

Test standards are firmly established models for comparison which serve certain test purposes, and are used in a specific way in well proven test procedures. Test patterns imply the design aspect of test figures, and are used as such, in a more flexible manner. Since there are no established test procedures available for our test task we will not distinguish between the terms "standard" and "pattern". The selection of the test figures and the corresponding test procedures should be done such that most of the previously mentioned errors (Chapter 2.1.) can be checked. The errors listed under Chapter 2.1.6. are not specifically addressed.

2.2.1. Standard test grid

This is the most popular test figure for geometrical tests of x, y-measurement systems. As shown in Figure 7, this device consists of a number of intersecting parallel lines. The grid points are regularly distributed and calibrated. Wild, Heerbrugg offers a very precise glass grid plate with a coordinate precision of the calibrated grid points of 0.5 μm. The grid points are distributed over an area of 24 x 24 cm^2. The line width is constant. The grid spacing is 2 cm in both directions. It allows for a check of the global positioning accuracy of the scanner. For details see Appendix A.1.
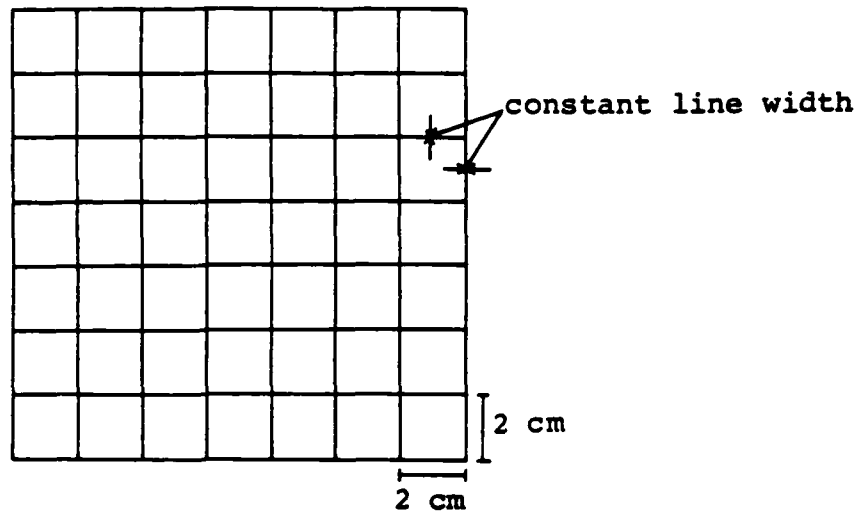
Figure 7: Standard test grid; constant line width, wide spacing

2.2.2. Square cross-line graticule

Similar to the standard test grid this device consists of two sets of parallel lines intersecting each other. However, the line widths are varying, the line distances are smaller and the overall size of the pattern is smaller.
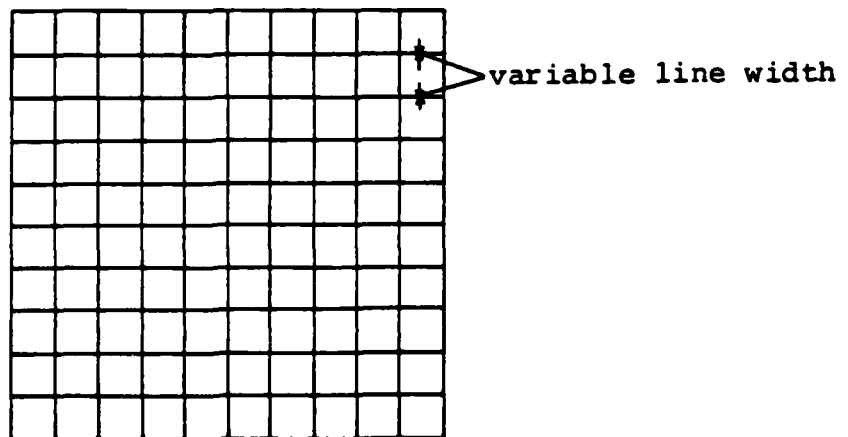
Figure 8: Square cross-line graticule; variable line width, narrow spacing

This device is readily available from Heidenhain in nine different versions. Three of them (nos. 14, 15, 16 for the different scanner resolution levels) could be considered here. See Appendix A.2.

2.2.3. Dot and line comparison

Appendix A.3. shows the dot and line comparison chart no. 20 from Heidenhain. The widths of the lines and the diameters of the dots range from 10 μm to 1000 μm. The spacing of the lines/dots of different widths is 2 mm. This chart can be used to check the resolution of individual fundamental patterns like single lines and dots. It can also be applied to check the local geometric performance of the scanner with respect to the rendering of these specific objects.

2.2.4. Parallel line test chart

The line test chart no. 32 from Heidenhain is shown in Appendix A.4. This chart with its variable line pitch can be used to check the length of the sensor array.

2.2.5. Radial circle test chart

This test chart is shown in Figure 9. It is not readily available, but it could possibly be manufactured by Heidenhain. This chart has the very desirable property of isotropy. The location of the center of the circles in the scanner output gives an indication of the local positioning accuracy. In addition the rendering of another fundamental object pattern, the circle, can be checked.
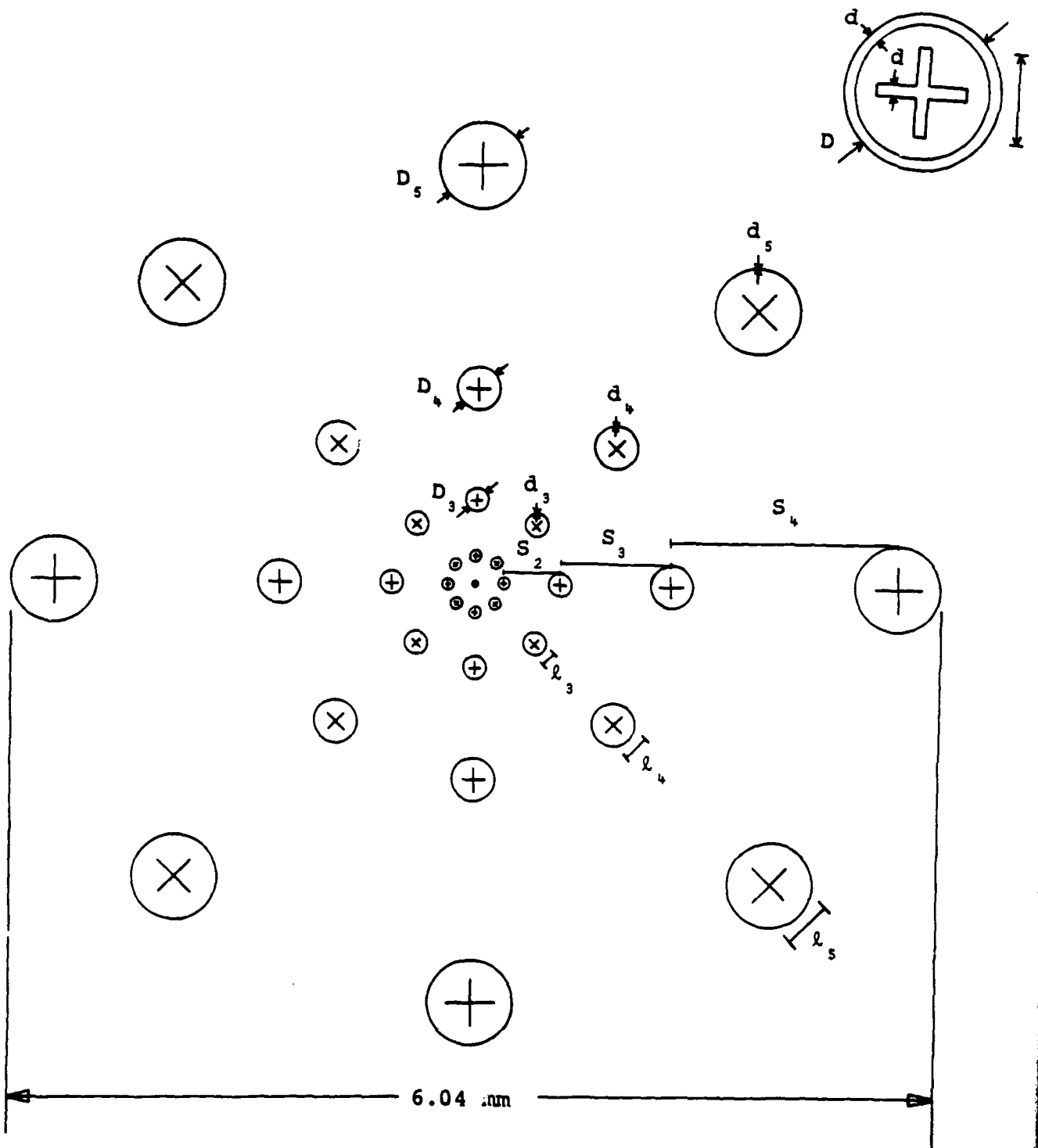
Figure 9: Radial circle test chart

<u>Dimensions of radial circle test chart figures</u>:

Distances of circles:	Diameters of circles:
$S_1 = 0.18$ mm	$D_1 = 35$ μm
$S_2 = 0.36$ mm	$D_2 = 70$ μm
$S_3 = 0.72$ mm	$D_3 = 140$ μm
$S_4 = 1.44$ mm	$D_4 = 280$ μm
	$D_5 = 560$ μm

Line widths:	Lengths of cross bars:
$d_1 = 5$ μm	$\ell_1 = 20$ μm
$d_2 = 10$ μm	$\ell_2 = 40$ μm
$d_3 = 20$ μm	$\ell_3 = 80$ μm
$d_4 = 40$ μm	$\ell_4 = 160$ μm
$d_5 = 80$ μm	$\ell_5 = 320$ μm

2.3. Test procedures, data processing, and data analysis

According to the purchase description of the AIDS (AIDS, 1982) a
display monitor and a cursor will be available to allow the operator to
perform measurements. The measurement resolution shall be one-third
pixel, which is well below the required one pixel positioning accuracy.
Since the scanner output data is in digital form the measurements could
either be performed in the digital domain or softcopies could be measured
using the monitor/cursor system. The latter option is preferred for the
geometrical tests because it does not require the extensive software which
would be necessary for the interpretation and measurement of digital data.
Any operator related subjectivity in the measurement process is part of
the system and would occur in the measurement of real photographs as well.
For the test purpose at hand an operator-driven measurement system is opti-
mal, it is flexible, fast, and inexpensive. For the radiometric tests it
is crucial to operate directly in the digital domain. Any intermediate
analog display of the digitized values would cause an additional modula-
tion and would require cascading.

The test figures suggested in Chapter 2.2. are gratings and grati-
cules on glass substrate. Since the AIDS can only scan film based ob-
jects the test figures have to be copied on film. It is suggested to use
Kodak High Resolution Duplicating Film (Ester Thick Base) SO-187 (see
Appendix B.1.). The film based test figures have to be measured on a
precision stereo-comparator or analytical plotter, stored and used under
constant humidity and temperature conditions. A possible distortion of
the test patterns, caused by a deformation of the film base/emulsion,
should be monitored through occasional remeasurements.

2.3.1. Test of the global geometric performance

This test uses the standard test grid described under 2.2.1. in order to determine the overall (global) geometric performance. The scanner output of the 13 x 13 = 169 crosses of the test grid is to be observed in two independent sets of measurements. It is suggested that the measurements be modelled by a bivariate, orthogonal polynomial. Bivariate orthogonal polynomials do have the following advantages compared to conventional polynomials:

- functional; bivariate polynomials compensate for the total deformation in all points of a regular grid if the order of the polynomial is adjusted to the number of grid points

- numerical; orthogonal polynomials produce optimal system stability; variances and covariances are minimal (Rao 1973, p. 235 ff)

- statistical; orthogonal polynomials lead to a higher power (type II error) in significance testing (Graybill 1961, p. 140)
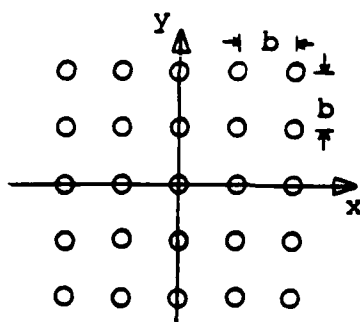
Figure 10:   5 x 5 = 25 grid point distribution

A bivariate polynomial, which is orthogonal with respect to a 5 x 5 = 25 regular grid point distribution (Figure 10) can be formulated as

$$\Delta x = \bar{y}^T A_5 \bar{x},$$
$$\Delta y = \bar{y}^T B_5 \bar{x} \tag{1}$$

with

$$\bar{y}^T = \begin{pmatrix} 1 & y^2 & (y^2-2b^2) & y(y^2- \frac{17}{5}b^2) & y^2(y^2- \frac{31}{7}b^2) + \frac{72}{35}b^4 \end{pmatrix}$$

$$\bar{x}^T = \begin{pmatrix} 1 & x^2 & (x^2-2b^2) & x(x^2- \frac{17}{5}b^2) & x^2(x^2- \frac{31}{7}b^2) + \frac{72}{35}b^4 \end{pmatrix} \tag{2}$$

and

$$A_5 = \begin{bmatrix} a_{11} & a_{12} & \cdots & a_{15} \\ \cdot & \cdot & \cdot & \cdot \\ \cdot & & \cdot & \cdot \\ \cdot & & & \cdot \\ a_{51} & a_{52} & \cdots & a_{55} \end{bmatrix} \;, \quad B_5 = \begin{bmatrix} b_{11} & b_{12} & \cdots & b_{15} \\ \cdot & \cdot & \cdot & \cdot \\ \cdot & & \cdot & \cdot \\ \cdot & & & \cdot \\ b_{51} & b_{52} & \cdots & b_{55} \end{bmatrix} \tag{3}$$

With the substitutions

$$k = x^2 - 2b^2, \quad \ell = y^2 - 2b^2, \quad p = x^2 - \frac{17}{5}b^2, \quad q = y^2 - \frac{17}{5}b^2,$$

$$r = x^2(x^2 - \frac{31}{7}b^2) + \frac{72}{35}b^4, \quad s = y^2(y^2 - \frac{31}{7}b^2) + \frac{72}{35}b^4 \tag{4}$$

we obtain

$$\Delta x = a_{11} + a_{12}x + a_{21}y + a_{22}xy + a_{13}k + a_{31}\ell + a_{23}yk + a_{32}x\ell +$$

$$+ a_{33}k\ell + a_{14}xp + a_{41}yq + a_{24}xyp + a_{42}xyq + a_{34}x\ell p +$$

$$+ a_{43}ykq + a_{44}xypq + a_{15}r + a_{51}s + a_{25}yr + a_{52}xs +$$

$$+ a_{35}\,r + a_{53}ks + a_{45}yqr + a_{54}xps + a_{55}rs \;;$$

$$\Delta y = b_{11} + b_{12}x + b_{21}y + b_{22}xy + b_{13}k + b_{31}\ell + b_{23}yk + b_{32}x\ell + \tag{5}$$

$$+ b_{33}k\ell + b_{14}xp + b_{41}yq + b_{24}xyp + b_{42}xyq + b_{34}x\ell p +$$

$$+ b_{43}ykq + b_{44}xypq + b_{15}r + b_{51}s + b_{25}yr + b_{52}xs +$$

$$+ b_{35}\,r + b_{53}ks + b_{45}yqr + b_{54}xps + b_{55}rs \;.$$

If the number of grid points is increased beyond 25 the property of orthogonality is lost, but even in this case the suggested polynomial is closer to orthogonality than a conventional polynomial.

If n grid points are used for polynomial coefficient determination, the average values of the observed grid point coordinates are computed as

$$x_{ij} = \frac{x'_{ij} + x''_{ij}}{2} \, , \qquad ', \, '' \, \ldots \text{ denotes first and second measurement cycle}$$

$$y_{ij} = \frac{y'_{ij} + y''_{ij}}{2} \, . \qquad i, j = 1, \ldots, n \tag{6}$$

The measurement precision is represented by the variances of the average values of two measurements.

$$\sigma_x^2 = \frac{1}{4n} \sum_{i,j} (x'_{ij} - x''_{ij})^2 \, ,$$

$$\sigma_y^2 = \frac{1}{4n} \sum_{i,j} (y'_{ij} - y''_{ij})^2 \tag{7}$$

The linear estimation model for the polynomial coefficients can be set up as

$$\begin{bmatrix} \Delta x \\ \Delta y \end{bmatrix} - \begin{bmatrix} \varepsilon_x \\ \varepsilon_y \end{bmatrix} = \begin{bmatrix} A_x & 0 \\ 0 & A_y \end{bmatrix} \begin{bmatrix} p_x \\ p_y \end{bmatrix} \; ; \qquad P = \begin{bmatrix} P_x & 0 \\ 0 & P_y \end{bmatrix} \tag{8}$$

with

$$\Delta x^T = (\overline{x}_{11} - x_{11}, \ldots, \overline{x}_{nn} - x_{nn})$$

$$\Delta y^T = (\overline{y}_{11} - y_{11}, \ldots, \overline{y}_{nn} - y_{nn})$$
... difference vectors of given and measured grid point coordinates

$\varepsilon_x, \varepsilon_y \ldots$ true error vectors

$P_x, P_y \ldots$ associated weight matrices

$p_x, p_y \ldots$ polynomial parameter vectors

$A_x, A_y \ldots$ associated design matrices

System (8) consists actually of two independent estimation models, which can be adjusted separately, as long as the joint weight matrix P has the blockdiagonal structure as indicated. In fact we are going a step further in assuming that P_x, P_y have diagonal structures with the diagonal elements derived from equation (7). The least squares approach leads thus to two sets of normal equations

$$N_x \hat{p}_x = L_x$$

$$N_y \hat{p}_y = L_y$$

(9)

with

$$N_x = (A_x^T P_x A_x)$$
$$N_y = (A_y^T P_y A_y)$$
$$L_x = A_x^T P_x \Delta x$$
$$L_y = A_y^T P_y \Delta y$$

Analysis of results:

The adjustment procedure will deliver the following values.

Estimated polynomial parameters:

$$\hat{p}_x = N_x^{-1} L_x \quad ,$$

$$\hat{p}_y = N_y^{-1} L_y \quad .$$

(10)

Residuals:

$$v_x = A_x \hat{p}_x - \Delta x \quad ,$$

$$v_y = A_y \hat{p}_y - \Delta y \quad .$$

(11)

Variances of unit weight:

$$\hat{\sigma}_{ox}^2 = \frac{v_x^T P_x v_x}{n - n_x} \quad ,$$

n_x, n_y ... number of polynomial parameters in p_x, p_y

$$\hat{\sigma}_{oy}^2 = \frac{v_y^T P_y v_y}{n - n_y} \quad . \tag{12}$$

Covariance matrices of the estimated polynomial parameters:

$$\Sigma_{p_x} = \hat{\sigma}_{ox}^2 N_x^{-1} \quad ,$$

$$\Sigma_{p_y} = \hat{\sigma}_{oy}^2 N_y^{-1} \quad . \tag{13}$$

Significance testing of polynomial parameters:

The test criteria

$$T_x = \frac{\hat{p}_x^T \Sigma_{p_x}^{-1} \hat{p}_x}{n_x}$$

$$T_y = \frac{\hat{p}_y^T \Sigma_{p_y}^{-1} \hat{p}_y}{n_y} \tag{14}$$

can be used to test whether the whole set of polynomial parameters is significant or not. Under the null-hypotheses

$$H_o^x : p_x = 0$$

$$H_o^y : p_y = 0 \tag{15}$$

the test criteria T_x, T_y follow the central Fisher distributions

$$T_x \sim F(n_x, n-n_x) \quad ,$$

$$T_y \sim F(n_y, n-n_y) \quad . \tag{16}$$

We reject H_0^x, H_0^y if

$$T_x > C_x = F(1-\bar{\alpha}, n_x, n-n_x), \quad \bar{\alpha} \ldots \text{ type I error size of the global tests}$$

$$T_y > C_y = F(1-\bar{\alpha}, n_y, n-n_y). \tag{17}$$

If any one of the global null-hypotheses (15) is rejected, the significance of the associated individual polynomial parameters should be tested. The probability levels of these individual tests are related to those of the general test. If the individual polynomial parameters would be independent of each other, the type I error size $\bar{\alpha}$ of the global tests would be related to the type I error sizes α_x, α_y of the individual tests according to:

$$(1-\bar{\alpha}) = (1-\alpha_x)^{n_x} \quad ,$$

$$(1-\bar{\alpha}) = (1-\alpha_y)^{n_y} \quad . \tag{18}$$

Strict orthogonality among the polynomial parameters is not valid any more if more than the necessary number of grid points (25 points in this example) is used. A solution to this problem is to orthogonalize the vector of polynomial parameters a-posteriori and to test the orthogonalized components. This can be achieved practically without any additional computational amount, if the solution of (9) is obtained by triangular factorization of N_x, N_y. The intention is to transform the original solution vectors $\hat{p}_x$, $\hat{p}_y$ (distributions: $\hat{p}_x \sim N(p_x, \Sigma_{p_x})$, $\hat{p}_y \sim N(p_y, \Sigma_{p_y})$) with the transformations

$$\hat{f}_x = F_x \hat{p}_x \quad ,$$

$$\hat{f}_y = F_y \hat{p}_y \quad ,$$

(19)

into orthogonal components $\hat{f}_x$, $\hat{f}_y$ with the distributions $\hat{f}_x \sim N(F_x p_x, \sigma_{0x}^2 Q_{f_x})$, $\hat{f}_y \sim N(F_y p_y, \sigma_{0y}^2 \hat{Q}_{f_y})$. It can be shown that F_x, F_y can be chosen such that $Q_{f_x} = Q_{f_y} = I$, so that the components of $\hat{f}_x$, $\hat{f}_y$ are independent on each other. If the normal equations matrices N_x, N_y are Cholesky-factorized with

$$N_x = C_x C_x^T \quad , \quad N_y = C_y C_y^T \quad ,$$

(20)

the system (9) takes the form

$$C_x C_x^T \hat{p}_x = L_x \quad ,$$

$$C_y C_y^T \hat{p}_y = L_y \quad .$$

(21)

or

$$C_x^T \hat{p}_x = C_x^{-1} L_x \quad ,$$

$$C_y^T \hat{p}_y = C_y^{-1} L_y \quad .$$

(22)

It can be shown (Finn 1974, p. 138) that the orthogonal components of $\hat{p}_x$, $\hat{p}_y$ are

$$\hat{f}_x = C_x^{-1} L_x \quad ,$$

$$\hat{f}_y = C_y^{-1} L_y \quad ,$$

(23)

which are the factorized "right hand sides" of the normal equations (9). These vectors are generated during the factorization procedure. All that is needed is to test their components.

Under the null-hypotheses

$$H_{ox}^{i} : \ f_{x_i} = 0 \ ,$$

$$H_{oy}^{j} : \ f_{y_j} = 0 \ ,$$

(24)

the corresponding test criteria

$$t_{x_i} = \frac{\hat{f}_{x_i}}{\hat{\sigma}_{ox}} \ ,$$

(25)

$$t_{y_j} = \frac{\hat{f}_{y_j}}{\hat{\sigma}_{oy}} \ ,$$

are Student-distributed with

$$t_{x_i} \sim t(n-n_x) \ ,$$

$$t_{y_j} \sim t(n-n_y) \ .$$

(26)

If

$$t_{x_i} \leqslant C_x = t(1-\alpha_x, \ n-n_x)$$

$$t_{y_j} \leqslant C_y = t(1-\alpha_y, \ n-n_y)$$

(27)

the null-hypotheses (24) are accepted.

In this case the corresponding components $\hat{f}_{x_i}$, $\hat{f}_{y_j}$ are set to zero ($\hat{f}_{x_i} = 0$, $\hat{f}_{y_j} = 0$). Finally the original polynomial parameters are computed by backsubstitution from

$$C_x^T \hat{p}_x = f_x' \ ,$$

$$C_y^T \hat{p}_y = f_y' \ ,$$

(28)

whereby f'_x, f'_y are the "cleaned" orthogonal parameter vectors. All other aspects of the data processing procedure are, for the most part, standard. Blunder detection can be performed by computing the residual vectors v_x, v_y and applying Baarda's data-snooping technique (compare e.g. Gruen, 1978). It may be of interest to investigate the type of deformation involved if only a three-parameter transformation is applied, i.e. two translation components and one rotation.

To achieve this, use the transformation:

$$\Delta x = \bar{y}^T A_{sr} \bar{x}$$

$$\Delta y = \bar{y}^T B_{sr} \bar{x} \tag{29}$$

with

$$A_{sr} = \begin{bmatrix} a_{11} & 0 \\ a_{21} & 0 \end{bmatrix} \quad , \quad B_{sr} = \begin{bmatrix} b_{11} & a_{21} \\ 0 & 0 \end{bmatrix} . \tag{30}$$

The adjustment is performed as previously outlined, except that the testing of parameters is not necessary in this case. Here the pattern generated by the residuals is of particular interest. It is suggested that the residuals v_x, v_y be plotted. A visual inspection of this plot will reveal any deformations. A scale factor in the data can be compensated by a similarity transformation. Two different scale factors along the coordinate axes and a shearing effect can be accommodated by an affine transformation. The formulae for these transformations are

similarity transformation:

$$\Delta x = \bar{y}^T A_s \bar{x}$$

$$\Delta y = \bar{y}^T B_s \bar{x} \tag{31}$$

with

$$A_s = \begin{bmatrix} a_{11} & a_{12} \\ -a_{21} & 0 \end{bmatrix} \quad , \quad B_s = \begin{bmatrix} b_{11} & a_{21} \\ a_{12} & 0 \end{bmatrix} \quad . \tag{32}$$

affine transformation:

$$\Delta x = \overline{y}^T A_a \overline{x}$$

$$\tag{33}$$

$$\Delta y = \overline{y}^T B_a \overline{x}$$

with

$$A_a = \begin{bmatrix} a_{11} & a_{12} \\ a_{21} & 0 \end{bmatrix} \quad , \quad B_a = \begin{bmatrix} b_{11} & b_{12} \\ b_{21} & 0 \end{bmatrix} \quad . \tag{34}$$

2.3.2. Skewness and linearity of the array line

Both errors can be checked by scanning one or more lines which are inclined to the scan direction. The standard test grid and/or the square cross-line graticule can be used for this purpose. The test figure should be mounted at the scanner stage such that one group of lines is approximately perpendicular to the scan direction. Visual inspection of the output for these lines would indicate a defect. The skewness of the array line would show up in a sawtooth shaped output line (Figure 11).
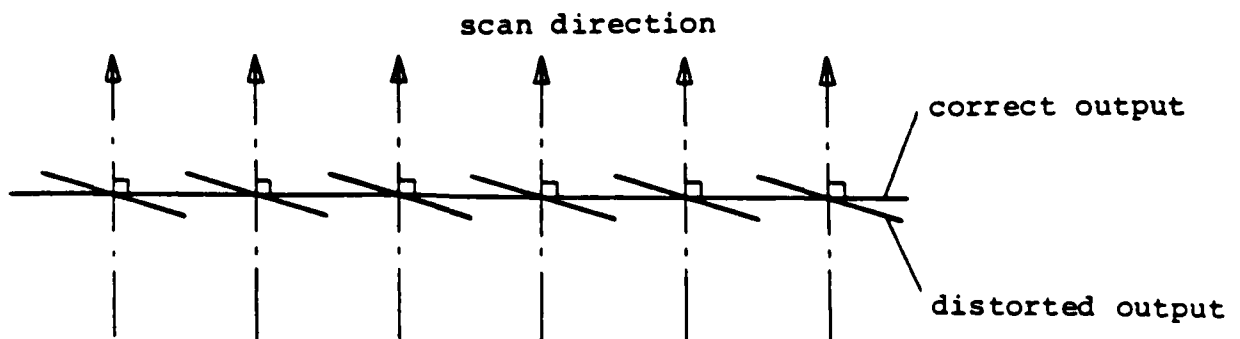
Figure 11: Effect of skewness of array line on output of test line perpendicular to scan direction

A non-linearity of the array line would result in a distortion of the test lines. The pattern of distortion would depend on the type of non-linearity. It would show up as a regular pattern with a spacing equal to the array length (similar to the skewness pattern).

2.3.3. Interval tracking error and length error of the array line

A constant interval tracking error (Chapter 2.1.1.) and a length error (Chapter 2.1.3.) of the array line can be separated from each other if the output of one single array line is extracted and analyzed. In order to check the length of the array line, the use of Heidenhain's test chart no. 32 (Appendix A.4.) is suggested. This chart should be scanned with the lines parallel to the scan direction. The difference between input and output line spacing gives directly an indication of an array line length error. The film based line test chart should be measured on a precision comparator or analytical plotter prior to the scanning process in order to verify the line widths and distances.

For the check of the constant interval tracking error the standard test grid and/or the square cross-line graticule can be used. The test figure should be set up such that one group of lines is parallel to the scan direction. The comparison between input and output distances between these parallel lines show the accumulated effect of this tracking error.

scan direction

d_i ... input distance

d_i' ... output distance

n_i ... no. of scan lines covering the distance

$$\Delta d_i = \frac{d_i - d_i'}{n_i} \; ;$$

$i = 1, \ldots, s$

grid lines s ... no. of distances

$\overline{\Delta d}$ ... constant interval tracking error

$$\overline{\Delta d} = \frac{\Sigma \Delta d_i}{s}$$

d_1

d_2

d_3
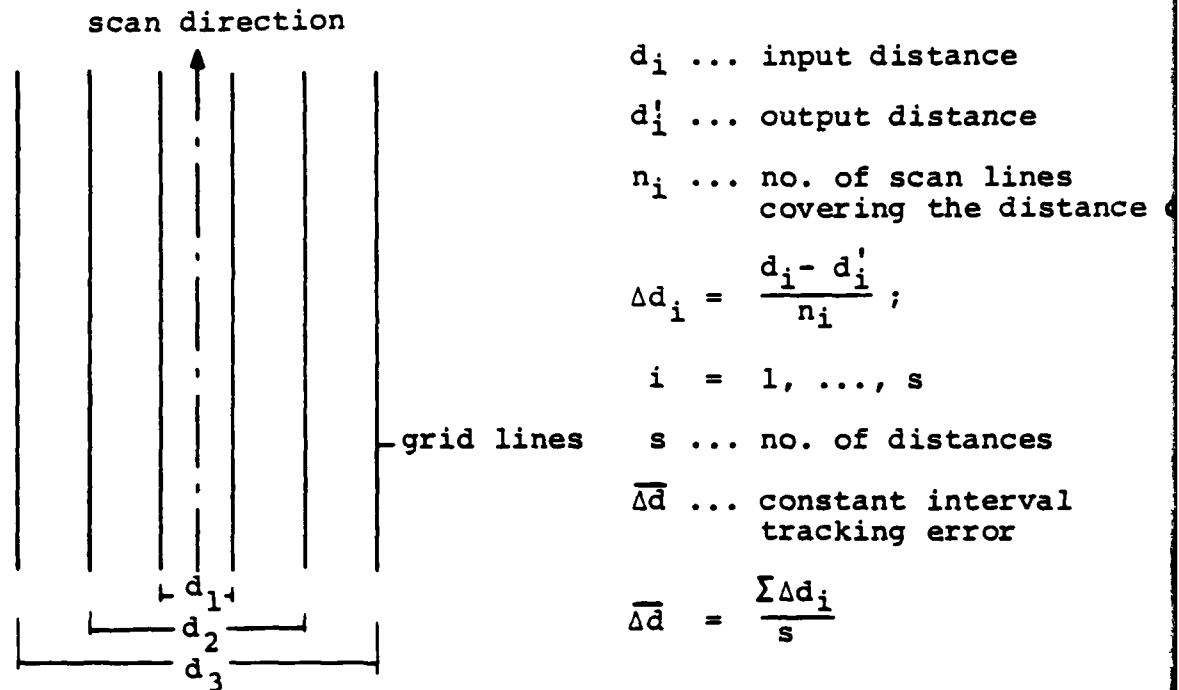
Figure 12: Determination of the constant interval tracking error

The non-constant portion of this tracking error can be checked if sets
of two adjacent scans are analyzed. This can be a very tedious proce-
dure if many scan lines are tested. The line test chart no. 32 (Appendix
A.4.) could be used for this purpose. If not removed, the error would
show up as part of the total error budget as computed under test 2.3.1.

2.3.4. Convergence/divergence tracking error

By monitoring the parallelism of the output of two parallel input
lines this type of error can be analyzed. The input lines should be
parallel to the scan direction. The test grid lines (Appendix A.1.) could
serve this purpose. Again the overall tracking error might be split up
into a constant portion and an irregular part. The constant portion can

be determined by computing the average γ-value ($\bar{\gamma}$) for each set of two adjacent lines (see Figure 13).

scan direction
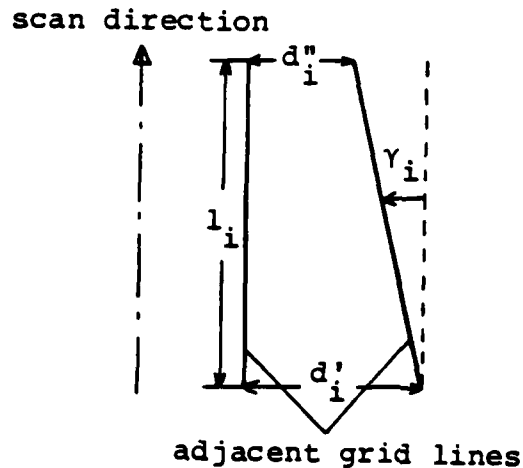
$$\gamma_i = \frac{d_i' - d_i''}{l_i}$$

$$i = 1, \ldots, s$$

s ... no. of line pairs used

$$\bar{\gamma} = \frac{\Sigma \gamma_i}{s}$$

adjacent grid lines

Figure 13: Determination of the constant convergence/divergence tracking error

For the monitoring of the non-constant portion we face a similar problem as under 2.3.3. Each pair of two adjacent lines must be investigated. A possible error of this type would show up in test 2.3.1.

2.3.5. Sampling rate error in scan direction

This error causes a scale change in the direction of scan and can be detected by checking the output distances between a set of parallel lines running perpendicular to the scan direction. The standard test grid lines can be used for this purpose. In addition, the global test 2.3.1. delivers the scale factor b_{21} in y-(scan) direction. A significant deviation of b_{21} from the value 1 would indicate a possible sampling rate error.

2.3.6. Stepping and waviness

These errors can be detected simply by checking the straightness of a standard test grid line in scan direction. A qualitative check can be performed visually. Measurements should be made only if these errors have to be quantized.

2.3.7. Local performance and rendering of fundamental patterns

In addition to a high geometrical positioning accuracy it is of vital importance for a precision scanner to render certain features accu·ately and completely. The most essential geometrical patterns, which form a basis for other more complicated features imaged on aerial photographs, are dot, circle, and bar. It is suggested that the output of the AIDS be checked with respect to the rendering of these patterns. The dot line comparison chart (Appendix A.3.) and the radial circle test chart (Figure 9) can be used as test standards. The radial circle test chart can also serve as a standard to check the local geometrical positioning accuracy. The standard test grid with its grid width of 2 cm can only control the global accuracy. The radial circle test chart with its 33 circles of different diameters and line widths, and with the center crosses spread point-symmetrically over a 6×6 mm^2 area, can control the local positioning accuracy. If the system works correctly, a 3-parameter transformation (equations (29), (30)) should be sufficient to connect the output coordinates of the crosses to the given, local values. Any additional significant polynomial terms indicate a malfunctioning.

3. Test of the radiometric performance

3.1. Introduction

The three basic image quality parameters that are used to describe the performance of a high speed film scanner-digitizer are MTF, linearity of response and noise level over the operating or dynamic range of the system. An additional parameter is the amount of flare or stray light present in the system. This was not specified in the AIDS purchase description but will be discussed later in this report. Three quantities that are seldom, if ever, specified are response uniformity, temporal stability and the influence of coherency effects on performance. These will also be discussed later in this report.

When considering MTF and response linearity one must be careful to evaluate the system at points throughout its scanning speed range as a function of target spatial frequency and for all outputs. (There will be only one output for a conventional microdensitometer type scanner, but there could be 2048 or more for a CCD system). Of particular concern here is the frequency response of the detector electronics, in particular the analog to digital (A/D) converter. Problems have been encountered with a scene dependent lag in response in the along-scan direction due to the Butterworth filter in the output of NASA's multi-spectral scanner system; four detectors in band 5 of the thematic mapper (TM) show an overshoot response when crossing a white-dark boundary, (Kieffer et al., 1983), and the PDS microdensitometer (Slater, 1980, pp. 388-394) exhibits a significant reduction in modulation output at scan speeds above 1 mm/s when scanning a 316 cy/mm target with a 1 μm scanning aperture, see Figure 19. The bin sizes (output level steps of the analog to digital converter) in the TM have been found to be unequal, which results in the histograms of uncorrected data from a random scene having a comb-like appearance rather than being smooth in shape. This problem reduces the quantization resolution from the advertized 8-bit to effectively 7-bit (Kieffer et al., 1983).
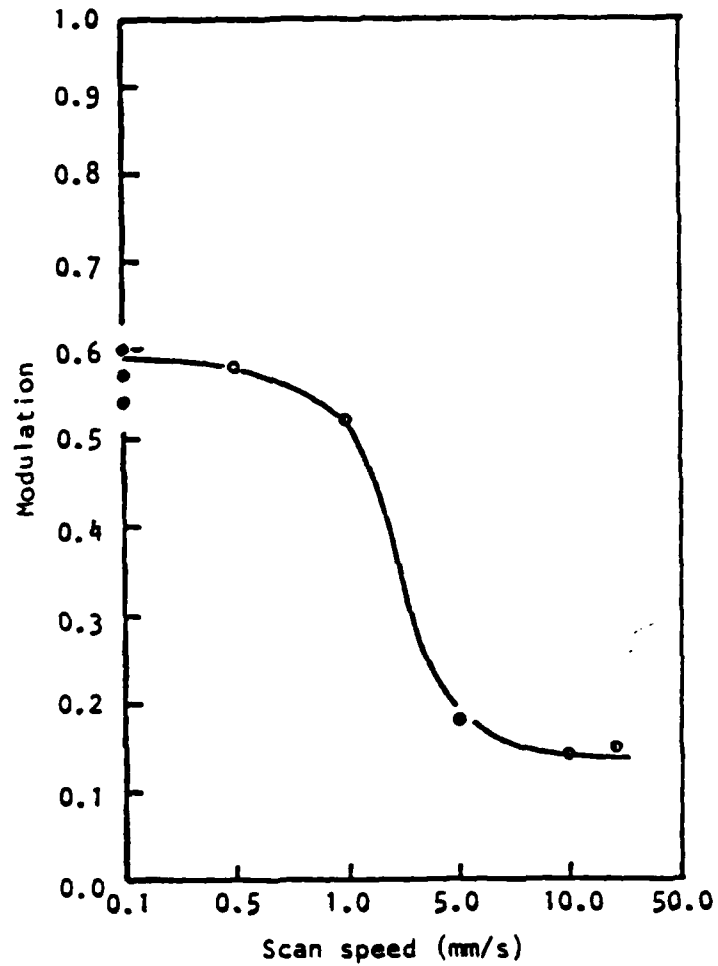
Figure 14: Scans to determine the effect of scan speed on recorded modulation. Conditions: 10X objectives; white light; 200X magnification; "A" apertures; 1-μm scanning aperture. Target frequency 316 cycles/mm

Although the reasons for some of these problems have not yet been fully determined, they relate, in the TM case, to the difficulty of sampling and digitizing some 4×10^6 point values per second. This is of the same order as the AIDS and two orders of magnitude higher than the PDS micro-densitometer. A second concern is that the response of the system be determined at various locations over the entire film format in order to check focus. The focus problem divides into four parts: First, the orthogonality of the film holder to the optical axis, second, the flat-ness of the film with respect to the holder, third, the parallelism of motion of the film holder, and fourth the quality of focus along the length of the scanning aperture. With an autofocus device, the first three may be insignificant but the sensitivity and frequency response of the auto-focusing need to be determined.

3.2. MTF measurement

There are two common ways to determine system MTF; the first is by reference to a square bar target array, the second is by edge gradient analysis. The former is simpler in terms of post-scan data processing but is more expensive because of the high quality resolution targets re-quired. Both methods will be described briefly in this section.

The bar target MTF can most conveniently be determined by use of a multibar target. Typically these are high or low contrast targets on film or glass that consist of sets of 15 light bars on a dark background as shown in Figure 15.

Group 1	Group 2	Group 3
1.00	10.00	100.0
1.26	12.59	125.9
1.58	15.85	158.5
2.00	19.96	199.6
2.51	25.12	251.2
3.16	31.63	316.3
3.98	39.82	398.2
5.01	50.14	501.4
6.31	63.13	631.3
7.95	79.48	794.8
10.00	100.00	1000.0

Figure 15: Example of 15-bar target

The choice of a 15-bar target is made for two reasons; first, it provides about 10 cycles, which are not distorted because of being near the ends of the pattern, to be averaged to get an accurate determination of modulation. Second, when scanned slowly, the focus can be easily adjusted to provide maximum modulation. This electrical focusing is more sensitive, repeatable and provides a higher modulation than visual focusing. Three-bar targets or continuously varying frequency targets do not have these advantages. Fifteen-bar targets, similar to those shown in Figure 15, can be produced on film. A set of standard 3-bar targets on 9.5 inch wide film in an arrangement suitable for AWAR (Area Weighted Average Resolution) testing has recently been sold to DMA by Itek Corp. according to Ron Carbonier of Itek (phone (617) 276-2551). He estimated that a similar arrangement of 15-bar targets covering the spatial frequency range 1-300 cy/mm would cost of the order of $2000.

In the particular example shown in Figure 15, in all but one case there are frequencies close to the specified values of 33, 50, 70 and 100 cy/mm. The MTF is found by scanning the target at the various frequencies up to as much as twice the frequency of interest. The modulation at each frequency is determined by the standard equation and the MTF curve is plotted

technique has been used extensively in the reconnaissance community (e.g. in 213] to determine overall in-flight system MTF. Thorough descriptions can be found in Thomas (1973), pp. 966-972 and Dainty, Shaw (1974), pp. 244-246.
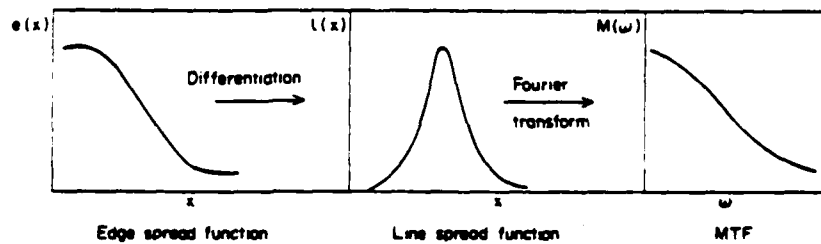
Figure 17: Derivation of the MTF from the edge response curve (after Dainty, Shaw, 1974, p. 245)

The first step in the procedure is to produce an extremely sharp edge between two large uniform areas of different densities. Usually the edge of a razor blade is contact printed onto an extremely high re-solving power film such as Eastman Kodak 649F, brush development is used to minimize adjacency effects. To calibrate the test edge function, a scan can be made with a 1 μm slit and a 1 um sampling interval using a high performance microdensitometer. A typical result is shown in Figure 18 of the spatial frequency of the edge as determined by an ⁻GA computer program (written by R.A. Schowengerdt at the University of Arizona). Corrections of this spectrum should be made for the width of the scan-ning slit using the sine function for the slit.

In the second step, the scanner/digitizer is used to scan the edge several times in both directions at different speeds to determine possible hysteresis effects (where the response is modified by the proceeding signal level) or frequency response deficiencies in the detector(s) and electronics. For this measurement, the scan direction should be accurately perpendicular to the straight edge.
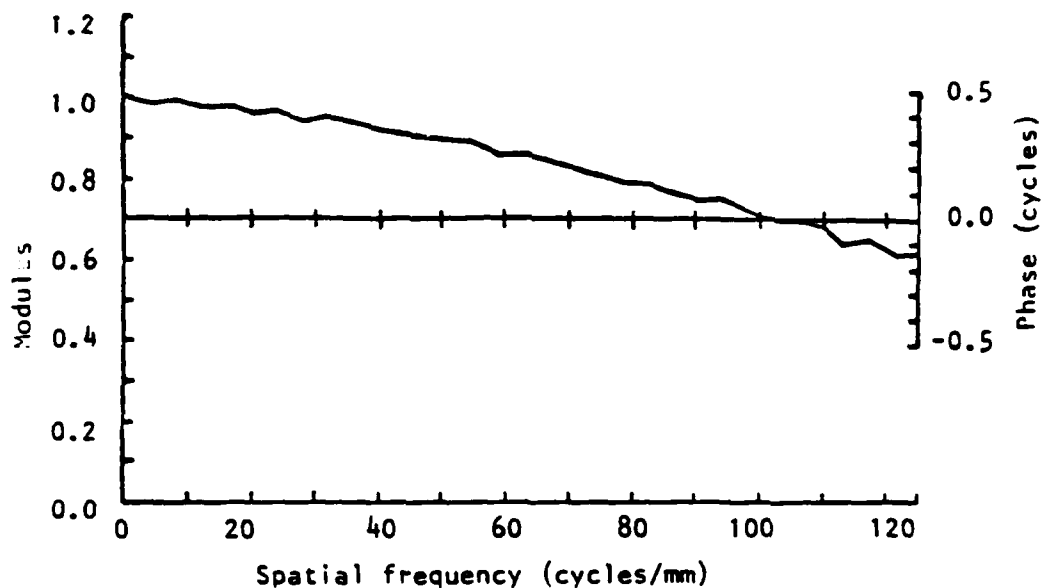
Figure 18: Calibration edge spectrum multiplied by microdensitometer OTF for 0.001 by 0.100-mm aperture

The third step is manually to draw a smooth curve through the edge trace or use a computer program to best-fit polynomials over the toe and shoulder of the curve. If the latter program written by Schowengerdt is used it will continue to plot the required square wave MTF, at whatever spatial frequency intervals are requested, by differentiating the smoothed edge trace and then taking the Fourier transform of the result. A manual approach is described in Thomas (1973), but for the purpose of evaluating AIDS, a computerized approach is recommended. Schowengerdt's program or software at 213 should be available.

Finally, the frequency spectrum of the edge should be accounted for by dividing the MTF obtained in step 3 by that spectrum.

In the data analysis step, if a CCD linear array is used, care should be taken to examine the output from all detectors. There can be significant differences from detector to detector as well as slowly varying changes in sensitivity across the array. Both of these can generally be

corrected to about the 0.1% level. In addition, the effect of scan speed and sampling frequency on MTF for each detector should be determined. <u>Even if the EGA method is not used for MTF determination, the edge response should be used for carefully checking response uniformity as a function of scan speed, sampling frequency and contrast</u>.

MTF curves obtained by the EGA method for a PDS microdensitometer are shown for various scan speeds, two scan directions and for two adjustments in Figures 19, 20 and 21.
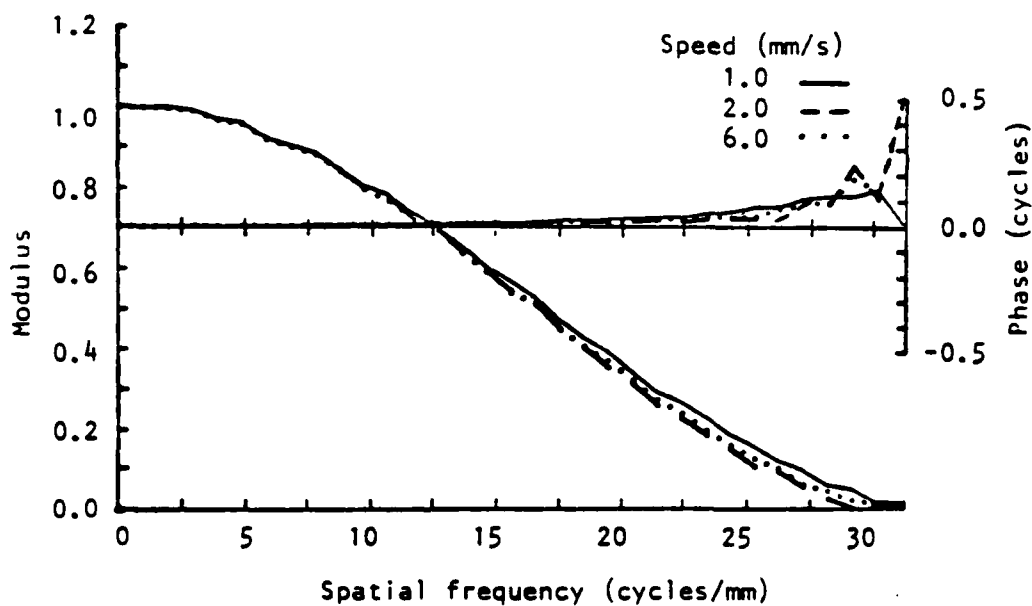
Figure 19: Microdensitometer OTF for different scan speeds for a 0.040-mm aperture
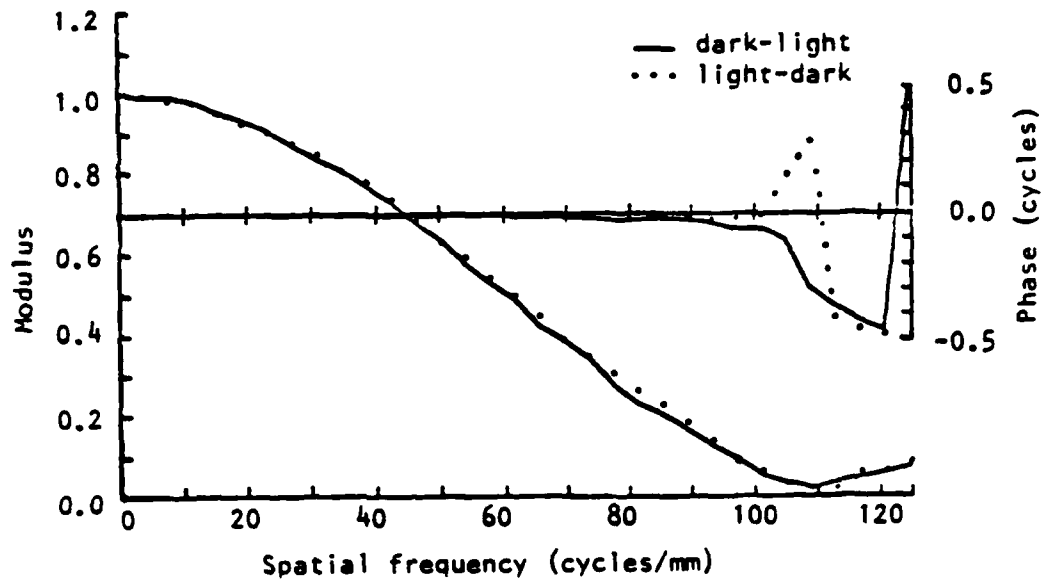
Figure 20: Microdensitometer OTF for opposite scan directions over edge for 0.010-mm aperture (scan speed = 0.3 mm/s)
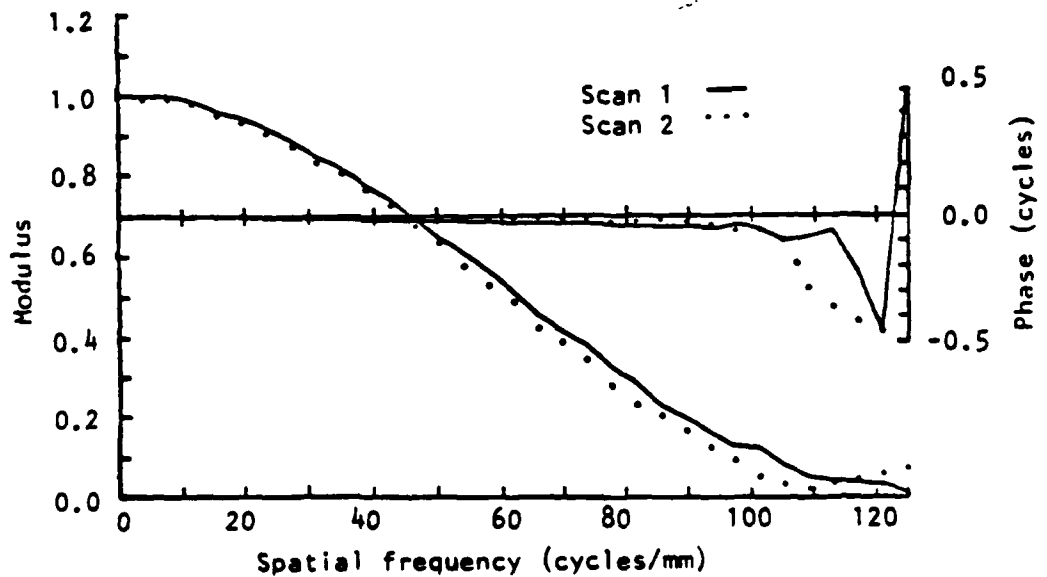
Figure 21: Microdensitometer OTF reproducibility for two independent alignments by same operator for 0.010-mm aperture

3.3. Dynamic range, linearity and noise

The purpose of the following test is to check the radiometric response of the AIDS while varying parameters such as dectector gain, aperture size and calibration neutral density filters (if included).

Two types of targets are available for this test. One is a grey step tablet available from Eastman Kodak that varies from clear to a density of 3.0 in about 20 steps. The other is a continuous grey scale that can be fabricated by grinding and polishing a wedge from a thick glass neutral density filter and then contact printing the wedge onto film.

Some results from tests on a PDS microdensitometer are shown in Figure 22. Note that this instrument uses a photomultiplier tube that has a larger dynamic range than CCD arrays and the non-linearity effects are only observable at very high and low light levels, when the applied PMT voltages were low and high respectively. For example, for the very large 40 x 400 μm slit with no ND filter (the fourth line down) the PMT voltage had to be set very low so as not to exceed the maximum signal out. This gave rise to a non-linear response over the 0-1.0 target density range. At the other extreme, the lowest fan of three lines covers the density range 5 to 7. Here the PMT voltage had to be set at its highest permissible level and not only was a non-linear response observed but also the effect of noise in the width of the fan. AIDS will not have to operate over a range of more than 0 to 2.5 density units so we might anticipate that non-linearity, noise and dynamic range would not be a problem. We should note, however, that the dynamic range of CCDs may be less than 1000:1 and that at high speeds the signal to noise ratio will be reduced because of the decreased integration time. Again these tests should be made as a function of scan speed and sampling rate.

The dynamic range and linearity test can be conducted with either the step tablet or the continuous wedge. Either should be checked with a PDS microdensitometer using a large aperture (say 40 x 200 μm). The linearity of the PDS can easily be checked by scanning a straight edge across the large aperture.
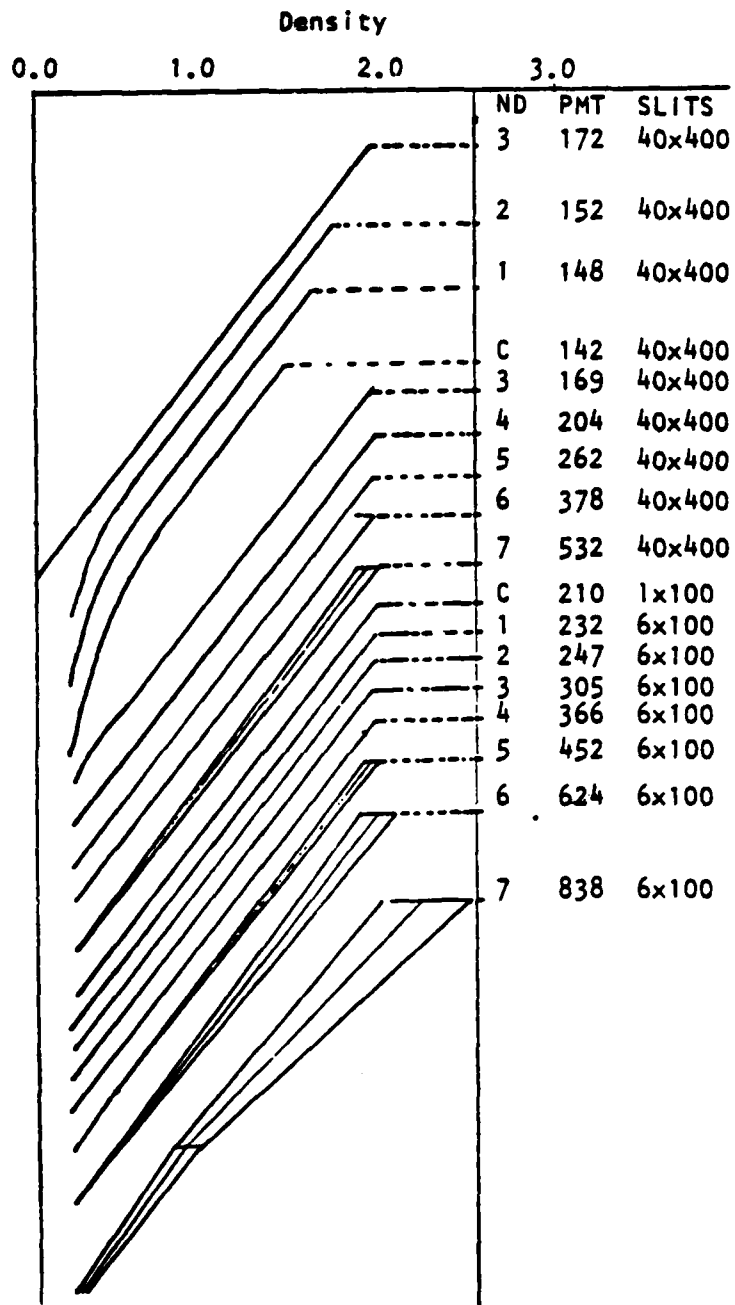
Figure 22: Linearity and noise as a function of neutral density, photo-multiplier tube voltage, and scanning aperture size

The use of the readily available Eastman Kodak 20-step tablet for the linearity test at the 0.5% level may be marginal. A tablet containing a larger number of steps can be readily fabricated in a photographic laboratory.

To determine the noise level of the system, and to avoid spatial variations in the filter being misinterpreted as noise, a 2.5 neutral density filter should be placed in the scanner at an out of focus location. With the system in the scanning mode, the noise of the output signal should be less than one quantization level, i.e., <0.1%.

3.4. Response uniformity

Response nonuniformities can be of two kinds. The response across any detector may be nonuniform or, if a detector array is used, there may be a detector-to-detector and/or a gradual response variation along the length of the array.

The first can be checked by scanning the array across a straight edge parallel to the length of the array. Any jaggedness in the output will indicate a nonuniform response, i.e., that there is a sensitivity difference between the leading and trailing edge of one or more detectors. This effect could introduce a significant mensuration error which would not necessarily be apparent from a measurement of the array geometry.

A variation in response along the length of an array can be corrected in post-scan signal processing; however, its magnitude has to be known. One method to accomplish this is to scan the length of an Eastman Kodak step tablet, monitoring the output of each detector at each density level. The two defects of detector-to-detector variations or striping and the gradual change over several hundred detectors will be apparent, particularly with 10-bit quantization. The latter can be a result of how the

detectors were fabricated and/or of the uneven illumination of the target to be scanned. Post-scan signal processing should reduce these nonuniformities to less than one quantization level, i.e., <0.1%.

3.5. Flare light

Permissible flare light level was not specified in the AIDS purchase description and for a well-designed fixed-aperture system may be of no consequence. For systems that provide various scanning aperture sizes and different sets of apertures, the amount of flare or stray light will depend on the choice of pre-aperture used with the selected post-aperture. In badly designed and/or dusty systems, the flare light can be substantial and significantly reduce the MTF. In such cases it may be possible to enhance performance by introducing flare stops in the system.

The effects of flare can be expressed quantitatively in terms of MTF reduction or arbitrarily in terms of the density measured when the scanning area is blocked by a microdot 2, 5 or 10 times its size.

Figure 23 shows plots of modulation versus square bar frequency for a PDS microdensitometer using the Itek target described in Figure 15. The curves show that increasing the size of the pre-aperture increases the amount of flare light in the optical system and substantially reduces the MTF.
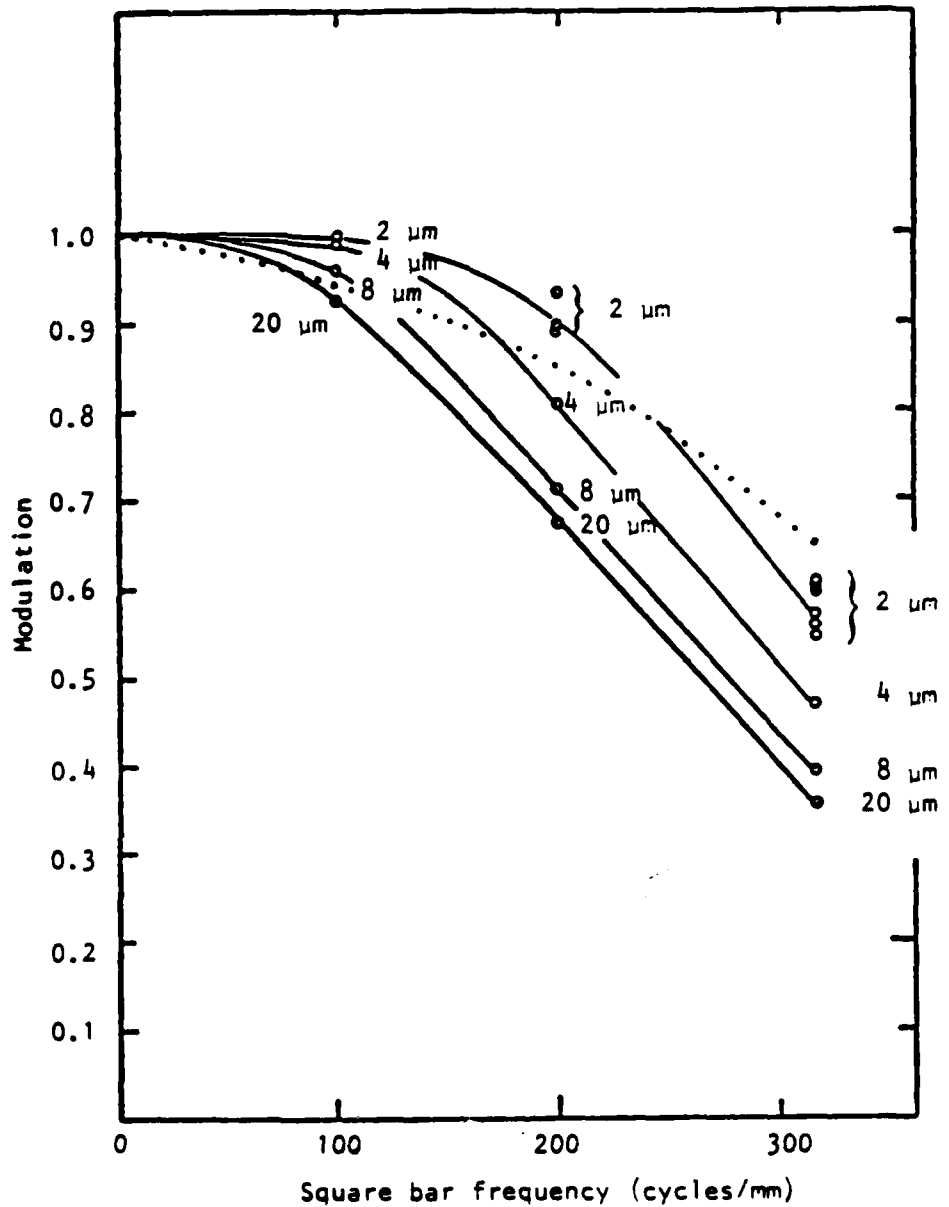
Figure 23: Scans to determine the influence of stray light on performance. Conditions: digital recording; 10X objectives; white light; 200X magnification; "A" apertures; speed 1 mm/s; 1-μm scan aperture. The numbers on the graph indicate the pre-aperture sizes. The dotted line is the incoherent, diffraction-limited square wave MTF (λ = 500 nm, NA = 0.25, post-aperture is 1 μm square)

3.6. Temporal stability

Temporal stability influences not only geometrical accuracy, but also radiometric accuracy. The problem usually results from the heat generated by the light source and electronics causing expansion or creep, during set-up and operation time, of one part of the optical system with respect to the other.

The PDS microdensitometer is, with its pre and post-apertures, particularly susceptible to thermal changes between parts of the instrument containing the two apertures. In a 12 hour period after turning on the light source the apertures moved apart by over 10 μm. The change in radiometric response is shown in Figure 24 over a 46 min. time period. Obviously, after the apertures, approximately 1 and 2 μm in size, had moved 1.5 μm with respect to each other, no light was transmitted and the density reading became very high.
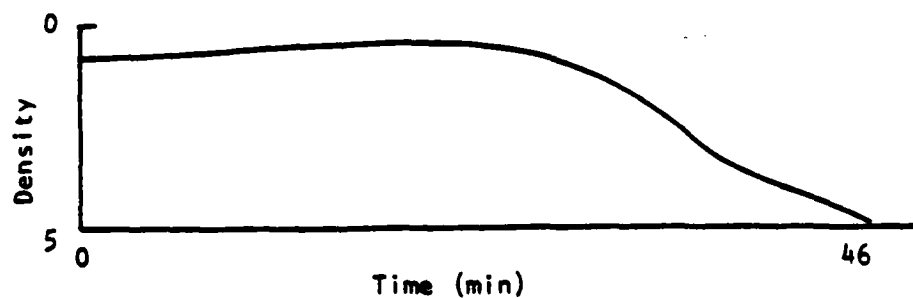
Figure 24: Density plot vs. warmup time

3.7. Coherency effects

Coherency effects are present in most microdensitometers and can only be minimized by collecting all the diffracted light transmitted by the target. If this is not achieved, density values will be high and depend on the phase structure of the target. Most processed film images show a relief image due to changes in film thickness caused by differential shrinkage of the image during processing.

Coherency effects often give rise to enhanced modulation. Thus the MTF curve for a perfect system shown as the dotted line in Figure 23 indicates that the 2-μm pre-aperature curve is higher than the perfect curve for spatial frequencies below 250 cy/mm. MTF curves generated this way are target dependent and only with a phaseless target can the true MTF be determined. Whether it is appropriate to measure the MTF with a phaseless target, or with a target produced on the same film to be routinely used with the system, is a matter for the buyer and seller to argue.

4. Test strategy

Because of the more critical nature of the radiometric performance it is suggested that the radiometric tests be performed prior to the geometric tests. Any necessary significant corrections to the radiometric components should be applied before entering the geometric test phase.

Table 1 gives a brief overview of the radiometric tests. Options are indicated and priorities marked.

The MTF determination, the check on dynamic range, response linearity and uniformity are absolutely necessary. These parameters are fundamental measures of the radiometric performance of the system. Flare light, temporal and coherency effects will influence those basic parameters. An independent determination of flare light, temporal and coherency effects becomes important, only if a thorough analysis of the system errors is required.

The spatial resolution is defined by the MTF curve and the specified threshold value of 0.3 for the modulus (AIDS, 1982). The resulting value is based on purely digital processing of the data. A visually determined spatial resolution might significantly deviate from this value. A threshold modulation curve for the display monitor would have to be used if resolution measurements are performed on this monitor.

Table 2 summarizes the geometric tests. Options and priorities are indicated.

The global and local geometrical accuracy tests are considered as absolutely necessary. If the system's output is congruent to the input a 3-parameter transformation (29) would be sufficient to relate corresponding input and output features to each other. Any additional significant polynomial term would indicate a malfunctioning. For the analysis of these possible additional polynomial terms the computation of the polynomial (1) for the global test should be done in two different ways. One computation should be based on the use of 5 x 5 grid and the true errors should be analyzed at the redundant grid points. The other should use the complete 13 x 13 grid for polynomial parameter determination. If the polynomial parameters of both methods are identical (within the range of random effects), it is safe to conclude that the system generates only global deformations. Otherwise, regional deformations are encountered and the modelling with global polynomials is not optimal.

A FORTRAN subroutine for the computation of bivariate orthogonal polynomials, based on a least squares adjustment as suggested in Chapter 2.3.1., is available in the Department of Geodetic Science and Surveying, OSU.

Another important procedure is the check on how fundamental objects like single bars, dots, and circles are rendered by the system. This can be considered as a variation of the standard resolution tests. The corresponding test standards are selected such that they can be used with variable scanner resolution.

Table 1: Radiometric tests

Test purpose	Test standards	Remarks	Priority
MTF determination	a) Itek 15-bar target b) Razor blade edge on Kodak 649F	Measurements as function of scan speed and position on the format; recording in-scan and across-scan direction; for CCD linear arrays: test of all detector outputs	1
Dynamic range, linearity, noise	a) Kodak grey step tablet b) Continuous grey scale	Measurements as function of scan speed and sampling rate	1
Response uniformity	Straight edge Kodak grey step tablet	Edge for nonuniformity across one detector; step tablet for variations along array line	1
Flare light	a) MTF reduction b) Microdot blocking	Amount depends on size of pre-aperture	2
Temporal stability	Neutral low density object	Compare density readings over a certain time period after switching on	2
Coherency effects	a) Phaseless target b) Standard film target	Optimal: Phaseless target	2

Table 2: Geometric Tests

Test purpose	Test standards	Remarks	Priority
Global performance	Wild standard test grid	a) 5x5 grid for polynomial coefficient determination; check true errors at other grid points after transformation b) 13x13 grid for polynomial coefficient determination c) 3-parameter, similarity, affine transformation with 13x13 grid	1
Local performance and rendering of fundamental objects	a) Dot and line comparison chart b) Radial circle test chart	Test standards designed for variable scanner resolution	1
*) Skewness and linearity of array line	a) Standard test grid b) Square cross-line graticule	Test lines inclined to scan direction; optimal: perpendicular	2
*) Length of array line	Line test chart (no. 32)	Analysis of output of a single array line	2
Stepping and waviness	Standard test grid	Qualitative check visually	2
Sampling rate error in scan direction	a) Standard test grid b) b_{21} coefficient from global test	Check of distance between parallel lines perpendicular to scan direction	2
Interval tracking error	a) Standard test grid b) Square cross-line graticule	Test lines parallel to scan direction Test chart no. 32 for non-constant portion	3
Convergence/ divergence tracking error	Standard test grid	Check of distance between parallel lines parallel to scan direction	3

*) ... applies to linear array scanners only

All the other geometrical tests are largely designed for the analysis of a possible malfunctioning, and as such for the detection of specific system errors.

5. Conclusions

For this report the test strategy of the AIDS scanner had to be set up as a device independent procedure. Because the final design of the system was not available all possible instrument errors could not be anticipated. Consequently the tests had to be constructed in a rather general way. Therefore it was appropriate to develop options and priorities, which are established in Chapter 4.

It is suggested that the radiometric tests be performed prior to the geometric tests. MTF determination, dynamic range, noise, linearity and uniformity of the detector response are considered as high priority tests. The tests on flare light, temporal stability, and coherency effects are second order tests. It is crucial that the measurements for the radiometric tests are performed directly with the digital data. The measurements for the geometrical tests should be performed on the display monitor. High priority geometrical tests are those on global performance, local performance and rendering of fundamental objects. The remaining tests of Table 2 are designed for the purpose of detecting specific instrument errors. Some of these tests, including length, skewness and linearity of array line, refer to the application of a linear array scanner. Some possible instrument errors like stepping, waviness, and tracking errors are easier to detect in linear array systems than in single element type scanners.

For the implementation of these test procedures and the processing of data, some computer programs are readily available from the Optical Sciences Center, University of Arizona, Tucson, and from the Department of Geodetic Science and Surveying, The Ohio State University, Columbus.

REFERENCES

Abrams, W.J., 1978: Performance evaluation of electro-optical focal
        planes for aerial reconnaissance. SPIE Vol. 137, Airborne Recon-
        naissance III, pp. 121-128.

AIDS, 1982: Purchase description for an advanced image digitizing sys-
        tem (AIDS). U.S. Army Engineer Topographic Laboratories, Fort
        Belvoir, VA, September 1982.

Bradley, W.C., 1978: Small geometry charge coupled devices for aerial
        imagery. SPIE Vol. 137, Airborne Reconnaissance III, pp. 116-120.

Dainty, J.C., Shaw, R., 1974: Image science. Academic Press, London,
        New York.

Finn, J.D., 1974: A general model for multivariate analysis. Holt,
        Richart and Winston, Inc., New York.

Graybill, F.A., 1961: An introduction to linear statistical models.
        Volume I. McGraw-Hill Book Company, Inc., New York.

Gruen, A., 1978: Accuracy, reliability and statistics in close-range
        photogrammetry. Proceedings of the Symposium of the Commission V
        of the ISP, Stockholm, August 1978.

Heidenhain, J.: Standard graticules. Brochure of DIADUR gratings. Dr.
        J. Heidenhain GmbH, Traunreuth; Heidenhain Corporation, 80 North
        Scott Street, Elk Grove Village, Illinois 60007, Tel. 312-593-6161.

Hoehle, J., 1983: Performance parameters of a digital plotting table
        for photogrammetry. Photogrammetric Engineering and Remote Sensing,
        Vol. 49, No. 1, pp. 111-118.

Hofmann, O., 1975: Geometric resolution and modulation transfer of photo
        sensors. In German. Bildmessung und Luftbildwesen, Vol 43, No. 5,
        pp. 174-181.

Hofmann, O., 1982: Digital recording technique. In German. Bildmessung
        und Luftbildwesen, Vol. 50, No. 1, pp. 16-32.

Hofmann, O., 1983: Image quality of active and passive scanners. In
        German. Bildmessung und Luftbildwesen, Vol. 51, No. 3, pp. 103-117.

Hofmann, O., 1983: Personal communications. Messerschmidt, Boelkow,
        Blohm, Ottobrunn.

Jones, R.J., 1976: Simulation of electro-optic image sensor performance.
SPIE Vol. 87, Advances in Image Transmission Techniques, pp. 88-108.

Kieffer, H.H., Eliason, E.M., Chavez, P.S., 1983: Thematic mapper intra-
band radiometric performance. Proceedings of Landsat-4 Early Results
Symposium, NASA Goddard Space Flight Center, February 1983.

Montuori, J.S., 1980: Image scanner technology. Photogrammetric Engi-
neering and Remote Sensing, Vol. 46, No. 1, pp. 49-61.

Purll, D.J., Smith, J.A., 1979: Evaluation of linear self-scanned imaging
arrays. ESA contract report, Sira Institute Ltd., South Hill Chisle-
hurst, Kent, England.

Rao, C.R., 1973: Linear statistical inference and its applications.
Second edition. John Wiley and Sons, New York.

Slater, P.N., 1980: Remote Sensing. Optics and Optical systems. Addison-
Wesley, Reading, Mass.

Thomas, W., 1973: SPSE Handbook of photographic science and engineering.
Wiley-Interscience.

Thompson, L.L., 1979: Remote sensing using solid-state array technology.
Photogrammetric Engineering and Remote Sensing, Vol. 45, No. 1, pp.
47-55.

Tracy, R.A., Noll, R.E., 1979: User-oriented data processing considera-
tions in linear array applications. Photogrammetric Engineering
and Remote Sensing, Vol. 45, No. 1, pp. 57-61.

APPENDICES

Appendix A.1: Standard test grid
                (available through Wild, Heerbrugg)

GRID PLATE TYPE No. 116 765

Position of 9 calibrated grid points as seen on the graduated surface

Serial No. of Plate

X

Y

Pl. No. 7019

500 mm

500 mm
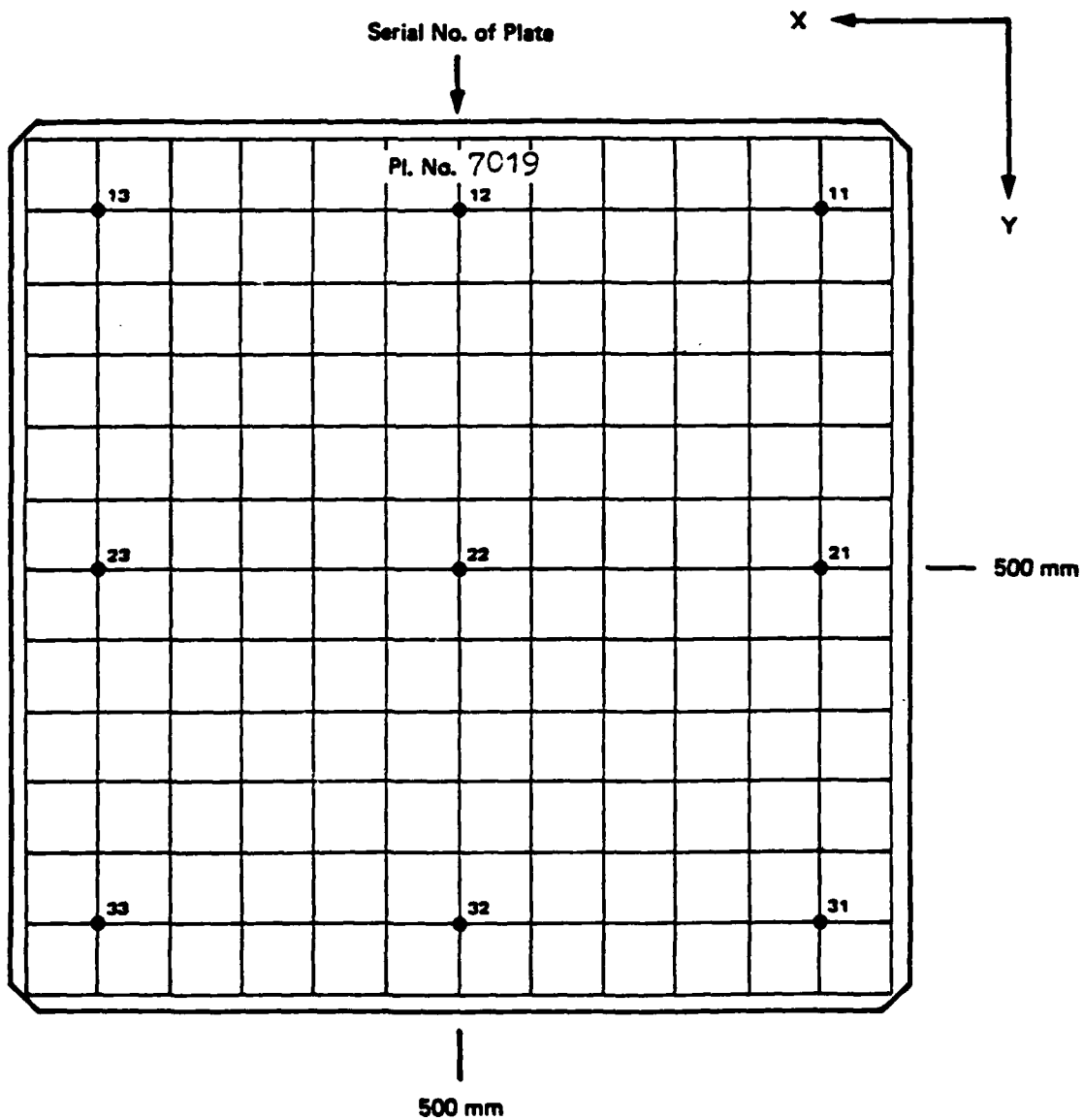
The coordinates listed on the attached sheet are given in millimeters, rounded to 10^{-3}mm.

The coordinate errors and the mean square errors of measurement (computed from differences of two independent sets of measurements) are given in microns (10^{-3}mm), rounded to the nearest tenth of a micron (10^{-4}mm).

GRID PLATE MEASUREMENT

EDV-NO.: 116765   PLATE-NO.: 7019   DATE: 80/05/13

FINAL COORDINATES (MM) AND ERRORS (MICROMETER):

POINT	X	DX	Y	DY
11	400.000	.4	400.000	.3
12	500.000	-.5	400.000	-.2
13	600.000	-.2	400.000	-.4
21	400.001	.6	499.999	-.8
22	499.999	-.5	500.000	-.5
23	600.000	-.1	500.000	.0
31	400.000	.5	600.000	.4
32	500.000	-.2	600.000	.2
33	600.000	-.0	600.001	.9

MSE OF MEASUREMENT : MX = .1 MY = .2
MSE OF COORDINATES : MO = .5

Appendix A.2: Square cross-line graticules (manufactured by Heidenhain)

14

1 mm-cross-line grid in DIADUR
Description: square cross-line grid
of 100 mm side length, divided into
squares of 1 mm side length.
Accuracy of graduation ± 15 μm.
Numerals are legible when viewed
through the glass.
Opaque lines on transparent background.
Glass substrate: 110×110×3 mm
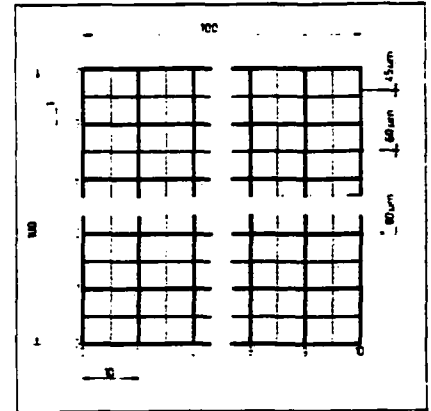
15a, 15b

1 2 mm-cross-line grid in DIADUR
Description: square cross- ne grid
of 75 mm side length, divided into
squares each of 0.5 mm side length.
Accuracy of graduation ± 10 um
Numerals are legible when viewed
through the glass.
Glass substrate: 85×85×3 mm

15a positive
opaque grating on
transparent background
15b negative
transparent grating on
opaque background
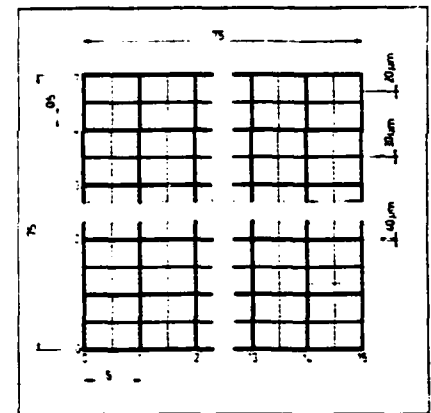
16

0.1 mm-cross-line grid in DIADUR
Description: square cross-line grid
of 50 mm side length, divided into
squares each of 0.1 mm side length
Accuracy of graduation ± 10 um.
Numerals are legible when viewed
through the glass
Opaque nes on a transparent
background.
Glass substrate: 60×60×3 mm
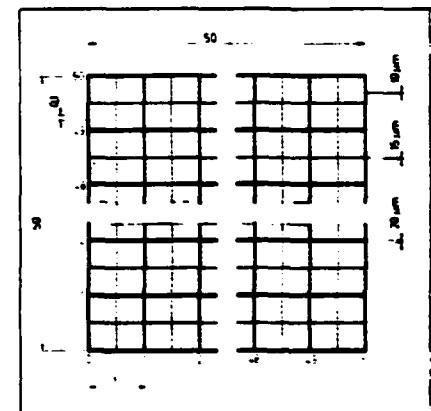
Appendix A.3:   Dot and line comparison chart
(manufactured by Heidenhain)

20a, 20b

Dot and line comparison chart from
10 μm to 1000 μm, **in DIADUR**
as item 19, but with two rows of 19 dots
and lines.
width/dia.
10, 20, 30, 40, 50, 60, 70, 80, 90,
100, 125, 150, 200, 250,
300, 400, 500, 750 and 1000 μm.
Glass substrate: 60×30×2 mm

20a positive:
opaque grating on
transparent background
20b negative:
transparent grating on
opaque background
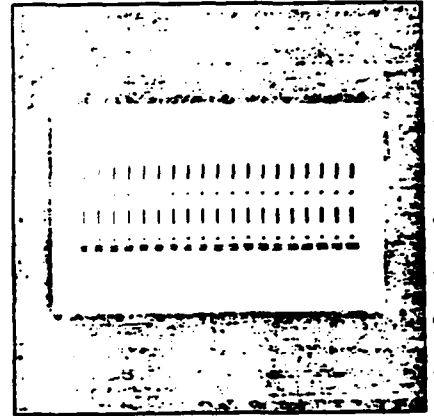
Appendix A.4:   Parallel line test chart
(manufactured by Heidenhain)

32

Line test chart in DIADUR
16 groups with line gratings
from 1.25 lines/mm up to 100 lines/mm,
i. e. grating pitch from 0.8 mm up to
0.01 mm, space to line ratio = 1 : 1
line length 22 mm
group lengths from approx. 2.4 mm up to
approx. 5 mm.
Opaque lines on transparent background.
Glass substrate: 85×35×3 mm.
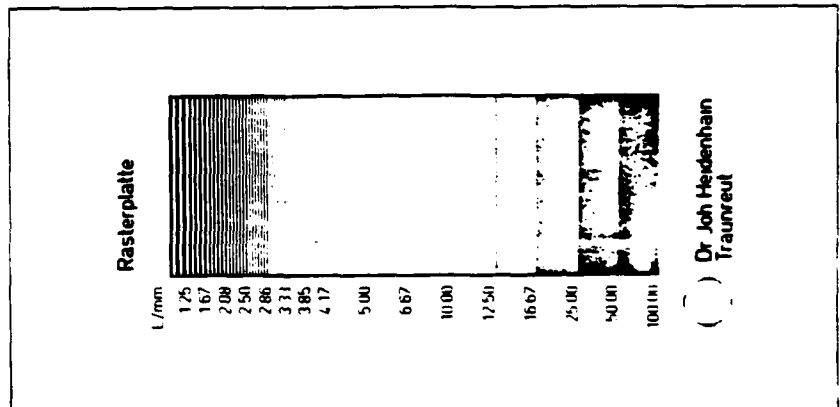
Appendix B: Kodak high resolution aerial duplicating film (Estar thick base) SO-187

SO-187/SO-192

KODAK HIGH RESOLUTION AERIAL DUPLICATING FILM (*ESTAR* THICK BASE) SO-187
KODAK HIGH RESOLUTION AERIAL DUPLICATING FILM (*ESTAR* BASE) SO-192

Blue-sensitive, extremely fine-grain negative films with very high resolving power. Designed for duplicating fine-grain aerial film.

Base:	SO-187: 7.0-mil EstAR Thick Base with a B-11 (fast-drying) backing. SO-192: 4.0-mil EstAR Base with a B-11 (fast-drying) backing.
Sensitivity:	Blue sensitive.
Safelight:	Use a KODAK Safelight Filter No. 1A (light red) in a suitable lamp with a 15-watt bulb at least 4 feet (1.2 metres) from the film.
Total Film Thickness:	SO-187: The nominal thickness of this film—including emulsion (0.26 mil), base (7.0 mils), and fast-drying backing (nil)—is 7.26 mils. SO-192: The nominal thickness of this film—including emulsion (0.26 mil), base (4.0 mils), and fast-drying backing—is 4.26 mils.
Gel/Base Ratio:	SO-187: 0.037 SO-192: 0.06
Weight:	SO-187: The weight of this film (unprocessed)—in equilibrium with 50 percent relative humidity—is 0.054 lb/ft² (0.027 g/cm²). SO-192: The weight of this film (unprocessed)—in equilibrium with 50 percent relative humidity—is 0.032 lb/ft² (0.016 g/cm²).
RMS Granularity Value:	5 (read at a net diffuse density of 1.0, 48-μm aperture).
Resolving Power:	Test-Object Contrast 1000:1—800 lines/mm Test-Object Contrast 1.6:1—250 lines/mm
Reciprocity Effect Adjustments:	For exposures in the range of 1/1000 to 1/100 second, no adjustments for reciprocity are required. For an exposure time in the range of 1/10 second, no adjustment in exposure time or development time is required. However, the lens aperture should be increased ½ stop. For an exposure time in the range of 1 second, no adjustment in development time is required. However, either the lens aperture should be increased 1 stop OR the exposure time should be increased to 2 seconds.